

USC: Uncompromising Spatial Constraints for Safety-Oriented 3D Object Detectors in Autonomous Driving

Brian Hsuan-Cheng Liao^{†‡}, Chih-Hong Cheng[§], Hasan Esen[†], Alois Knoll[‡]

Abstract—We consider the safety-oriented performance of 3D object detectors in autonomous driving contexts. Specifically, despite impressive results shown by the mass literature, developers often find it hard to ensure the safe deployment of these learning-based perception models. Attributing the challenge to the lack of safety-oriented metrics, we hereby present uncompromising spatial constraints (USC), which characterize the predictions to fully cover the objects when seen from the autonomous vehicle. The constraints, as we formulate using the perspective and bird’s-eye views, can be naturally reflected by quantitative measures, such that having an object detector with a higher score implies a lower risk of collision. Finally, beyond model evaluation, we incorporate the quantitative measures into common loss functions to enable safety-oriented fine-tuning for existing models. With experiments using the nuScenes dataset and a closed-loop simulation, our work demonstrates such considerations of safety notions at the perception level not only improve model performances beyond accuracy but also allow for a more direct linkage to actual system safety.

I. INTRODUCTION

3D object detection is an essential function for scene understanding in autonomous driving (AD). It allows an autonomous vehicle (AV) to locate objects in a scene and classify them into different categories so that the AV can navigate through them effectively.

In the past years, computer vision and deep learning literature have contributed greatly to the growing performances of 3D object detectors. More recently, aiming at wider and safer deployment of AVs, several works have adapted the general literature and designed performance indicators that consider driving dynamics. For example, instead of the generic Intersection-over-Union (IoU) measure, the nuScenes benchmark uses translation errors (TE) to match the predictions and ground truths and calculates several true-positive metrics for more fine-grained evaluation [1]. While various driving-oriented metrics are proposed, one challenge still remaining is the definition of a straightforward criterion, i.e., what score a model should attain to be satisfactory and deployable. Lately, the mitigation of the challenge has become more urgent, as regulations such as the EU AI Act [2] require developers to demonstrate “an appropriate level of performance” before marketing their solutions.

[†]Brian Hsuan-Cheng Liao and Hasan Esen are with DENSO AUTOMOTIVE Deutschland GmbH, 85386 Eching, Germany. h.liao@denso.eu, h.esen@denso.eu

[§]Chih-Hong Cheng is with the Department of Computer Science and Engineering, Chalmers University of Technology, 41296 Göteborg, Sweden chihhong@chalmers.se

[‡]Brian Hsuan-Cheng Liao and Alois Knoll are with the Department of Informatics, Technical University of Munich, 85748 Garching, Germany. knoll@in.tum.de

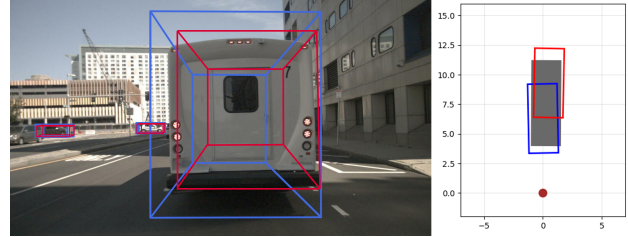


Fig. 1: An example scene that motivates our safety-oriented spatial constraints. For both the blue and the red predictions, $\text{IoU} \approx 0.7$ and $\text{TE} \approx 1.6$ (m) indistinguishably. We thereby focus on the objects’ nearest sides from the AV and propose USC. Effectively, the blue prediction has $\text{USC} = 1$, while the red one gets $\text{USC} \approx 0.8$.

Hence, in this work, we consider tolerable errors for 3D object detectors from a safety point of view and propose uncompromising spatial constraints (USC) as potential bottom lines. Concretely, *pivoting on object response and collision avoidance*, we underpin a requirement that states an object detector’s prediction should fully cover its corresponding ground truth when seen from the AV’s location. The reason is that such full coverage shall (already) result in a low risk of collision at the object’s edges close to the AV. Fig. 1 shows an example scene and contrasts USC with existing practices, which generally demand perfect alignment between the prediction and the ground truth.

More technically, when characterizing the requirement, we utilize perspective-view (PV) and bird’s-eye-view (BEV) projections to decompose the 3D predictions and ground truths into 2D representations. Such decomposition facilitates the definition of USC and, more importantly, leads to quantitative measures that allow us to assess different models at a finer scale. Notably, while the PV typically captures rich information for AD as shown by the prior art [3], [4], we point out the necessity of BEV constraints for the required full coverage. Moreover, beyond assessment, we exploit the quantitative measures and formulate a safety-oriented loss function to improve existing models.

To demonstrate the effect of our proposals, we conduct three sets of experiments with state-of-the-art models hosted on the MMDetection3D platform. First, we evaluate several models in the nuScenes dataset and check for safety concerns via USC-based metrics. We then improve one of the models through the safety-oriented loss function. Finally, by running the object detectors with an automatic emergency braking (AEB) function in a closed-loop setup, we show a better correlation with the AV’s collision rates enabled by USC. Altogether, our work serves as an initiative to address safety

principles and remedies for imperfect 3D object detectors in autonomous driving systems.

II. RELATED WORK

Object detection has attracted great research attention over the past two decades. Readers may refer to a recent survey that delineates the development [5]. In the following, we focus on the studies that concern AD and safety.

As one of the early results, Cheng et al. proposed a conceptual safety-aware hardening framework for object detectors [6]. Specifically, the authors defined a distance-based criticality criterion and adapted the NN architecture of a baseline model to enhance its performance in critical zones. Based on a similar idea, Lyssenko et al. refined the definition of criticality by considering object dynamics and improved pedestrian detection accordingly [7]. While these results contributed to better classification and detection of safety-critical objects generally, our study complements them by precisizing localization requirements at a finer scale. In fact, the introduced nuScenes benchmark lies in this direction [1]. It adopts the NuScenes Detection Score (NDS), computing not only the conventional mean average precision (mAP) metric [5] but also true-positive error measures on the localization function. Concurrently, Phillion et al. proposed planner-centric metrics, which compute the KL-divergence between the motion planning outcomes (i.e., trajectory waypoints) based on predictions and ground truths respectively [8]. Although the latter approach appears plausible, a recent validation work interestingly found NDS better correlating with actual AV collision rates, indicating the advantage of true-positive error measures at the object detection model level [9]. Hence, our investigation follows this direction, but as we shall see, while NDS demands perfectly aligned predictions, our work focuses on safety-oriented principles.

In the most recent literature, there exist several similar efforts. For instance, Deng et al. proposed Support Distance Error (SDE), computing the marginal gaps on the edges of a prediction and its targeted ground truth [10]. Their proposal, however, is tailored for a point cloud-based object representation in the BEV plane. Similarly, Mori et al. considered several safety-oriented adaptations for existing evaluation protocols, e.g., by redefining the shortest distance between two bounding boxes [11]. They also derived pass/fail criteria based on human perception performance. While the analysis with human benchmarks has been shown feasible, some considerations may be overly complicated, as reported in the work itself. Henceforth, we address localization constraints that are simplistic and general for 3D object detectors using the typical bounding box-based representation.

Lastly, there have also been interesting results that compensate for the imperfection of learning-based models. For example, De Gerancey et al. leveraged conformal prediction to post-process the predicted bounding boxes and obtain a statistical performance guarantee in ground truth alignment [3]. Similarly, Schuster et al. analytically derived a minimum multiplicative factor for enlarging the predictions so as to properly enclose the ground truths [4]. While these

results focus on the 2D image plane, our work distinctively targets 3D object detection, which is more directly linked with AD applications, and improves the models in a continual learning fashion.

III. PRELIMINARIES

As the foundation of our work, we further introduce the mostly adopted practices for object detector evaluation, including the typical IoU-based approach [5] and nuScenes' protocol [1].

For 3D object detection in AD, the common practice is to abstract objects with upright 3D bounding boxes [5]. It also usually assumes the AV at the origin $O(0, 0, 0)$ and a right-handed coordinate system with the z -axis parallel to the AV's heading and x pointing to the right. Then, an object's bounding box, taken as the ground truth, is annotated by a tuple $\hat{\mathbf{G}} \stackrel{\text{def}}{=} (x_{\mathbf{G}}, y_{\mathbf{G}}, z_{\mathbf{G}}, l_{\mathbf{G}}, h_{\mathbf{G}}, w_{\mathbf{G}}, \theta_{\mathbf{G}})$. Here, $x_{\mathbf{G}}, y_{\mathbf{G}}, z_{\mathbf{G}}$ are the center coordinates, $l_{\mathbf{G}}$ is the length (parallel with the x -axis when the orientation of the box is 0), $h_{\mathbf{G}}$ is the height (along the y -axis), $w_{\mathbf{G}}$ is the width (along the z -axis), and $\theta_{\mathbf{G}}$ is the rotation around the y -axis. Similarly, a prediction given by the object detector is represented by $\hat{\mathbf{P}} \stackrel{\text{def}}{=} (x_{\mathbf{P}}, y_{\mathbf{P}}, z_{\mathbf{P}}, l_{\mathbf{P}}, h_{\mathbf{P}}, w_{\mathbf{P}}, \theta_{\mathbf{P}})$.

Now, for assessing a prediction against a given ground truth, most studies use the IoU measure [5]. For its calculation, the 3D cuboids of the prediction and the ground truth, denoted as $\mathbf{P} \subset \mathbb{R}^3$ and $\mathbf{G} \subset \mathbb{R}^3$, are first reconstructed from the tuple representations through their corners. Then, IoU is defined as:

$$\text{IoU}(\mathbf{P}, \mathbf{G}) \stackrel{\text{def}}{=} \frac{\text{Vol}(\mathbf{P} \cap \mathbf{G})}{\text{Vol}(\mathbf{P}) + \text{Vol}(\mathbf{G}) - \text{Vol}(\mathbf{P} \cap \mathbf{G})}, \quad (1)$$

where $\text{Vol}(\cdot)$ is the volume of a given polyhedron, and $\mathbf{P} \cap \mathbf{G}$ denotes the intersection of the prediction \mathbf{P} and ground truth \mathbf{G} . For \mathbf{P} and \mathbf{G} , the volume can be easily computed with their dimensions (i.e., length, width, and height). For the intersection $\mathbf{P} \cap \mathbf{G}$, one normally derives its projected area in the BEV plane as well as its height along the z -axis separately and then multiplies them together to get the volume. In practice, there are advanced algorithms and software packages such as PyTorch3D [12] to implement the functions.

With the IoU's definition, more conventional protocols traverse the object classes and assess the set of predictions against all the ground truths per class [5]. Then, based on given IoU thresholds, the predictions are matched with the ground truths and grouped into true positives (TPs), false positives (FPs), and false negatives (FNs), whose counts are in turn used to compute recall, precision, and the mean Average Precision (mAP) metric. By contrast, the nuScenes benchmark adopts thresholds based on BEV center distances when calculating mAP and defines the more fine-grained NuScenes Detection Score (NDS) as follows:

$$\text{NDS} \stackrel{\text{def}}{=} \frac{1}{10} [5 \cdot \text{mAP} + \sum_{\text{TP} \in \text{TPs}} (1 - \min(1, \text{TP}))], \quad (2)$$

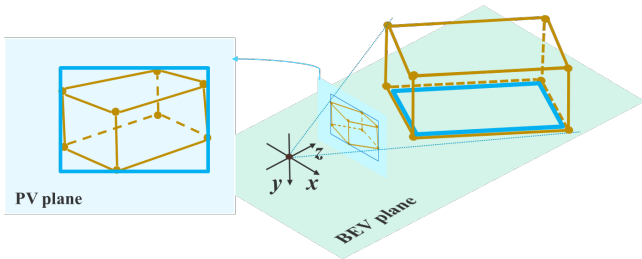


Fig. 2: We transform 3D bounding boxes into the PV and BEV planes for establishing USC and corresponding quantitative measures.

where $\mathbb{T}\mathbb{P}\mathbb{S}$ denotes the set of five TP measures for matched predictions and ground truths, concerning translation, orientation, scale, velocity, and attribute predicting errors. To be specific, the BEV center distance and the TP translation error (TE) between a prediction and a ground truth can be calculated with their representation attributes:

$$\text{TE}(\hat{\mathbf{P}}, \hat{\mathbf{G}}) = \sqrt{(x_{\mathbf{P}} - x_{\mathbf{G}})^2 + (z_{\mathbf{P}} - z_{\mathbf{G}})^2}. \quad (3)$$

For each class, TE is computed for all matched pairs and summarized into an *average TE* (ATE) score. Other TP measures follow the same process. For their definitions, readers are deferred to the nuScene benchmark [1].

As introduced, the IoU measure provides a generic indication of how well the prediction is aligned with the ground truth. Likewise, while NDS undertakes several driving-related considerations, it still regards errors from different directions equally and requires perfect predictions. We now present our safety-oriented spatial constraints which are motivated by error-tolerating considerations for collision avoidance from the AV's perspective.

IV. SAFETY-ORIENTED SPATIAL CONSTRAINTS

To iterate, our goal is to formulate uncompromising spatial constraints (USC) that ensure a given prediction \mathbf{P} fully covers the ground truth \mathbf{G} from the AV's perspective. Technically, as Fig. 2 depicts, we transform them into the PV and BEV planes, which are easier to handle than the direct 3D world. In the following Sec. IV-A, we first address PV which naturally reflects driving situations. Then, as PV foregoes the important depth information, we consider additional BEV constraints in Sec. IV-B. Finally, Sec. IV-C consolidates the respective PV and BEV constraints for comprehensive model evaluation.

A. Box Enclosure in the PV Plane

To formulate the spatial constraint in the PV plane, we first have to take a perspective projection for the prediction \mathbf{P} and the ground truth \mathbf{G} . This can be done straightforwardly for camera-based object detectors with the camera parameters and images. As for lidar-based models, one may borrow the camera system in the sensor suite or simply apply a pinhole-based perspective projection using a focal length $f = 1$. This is because our following analysis only considers the relative position and size of the projected prediction and ground truth.

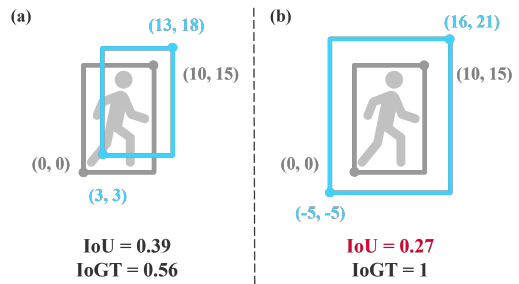


Fig. 3: A comparison of IoU and IoGT using the same ground truth (gray) and different predictions (blue) in (a) and (b). The prediction in (b) should be indicated as better than the one in (a) when considering collision avoidance. However, the IoU in (b) is lower, falling short to reflect the notion of “enclosure”.

As long as the same perspective projection (with any f) is applied to both the prediction \mathbf{P} and the ground truth \mathbf{G} , we can examine their relation in the PV plane. To elaborate, for a point $p(x_p, y_p, z_p)$ in the 3D world, one can obtain its coordinates (a, b) in the PV plane with the projection formula [13], written as:

$$\begin{bmatrix} a \\ b \\ f \end{bmatrix} = \frac{f}{z_p} \begin{bmatrix} x_p \\ y_p \\ z_p \end{bmatrix}. \quad (4)$$

The magnitude of the coordinates (a, b) depend on the focal length f , but, as mentioned, it will be the same for all points in the prediction \mathbf{P} and the ground truth \mathbf{G} .

Practically, as shown in Fig. 2, one only needs to consider the extreme points, i.e., the eight corners, of a 3D bounding box when performing the PV projection [14]. As the eight corners result in eight points in the PV plane, an axis-aligned bounding box can finally be constructed by finding the minimum and maximum coordinates in the vertical and horizontal axes respectively. In this way, we obtain the projected prediction \mathbf{P}^{PV} and ground truth \mathbf{G}^{PV} .

As studied in [3], [4], we can now formulate a direct constraint in the PV plane that requires the prediction \mathbf{P}^{PV} to fully enclose the ground truth \mathbf{G}^{PV} , i.e.,

$$\mathbb{I}^{\text{PV}} \stackrel{\text{def}}{=} \mathbf{G}^{\text{PV}} \subset \mathbf{P}^{\text{PV}}. \quad (5)$$

Intuitively, without a proper enclosure, the AV risks a higher chance of bumping into the object on its sides. For a quantitative characterization, the previous work [3], [4] adopted the IoU function in 2D. However, we find Intersection-over-Ground-Truth (IoGT) more suitable here:

$$\text{IoGT}(\mathbf{P}^{\text{PV}}, \mathbf{G}^{\text{PV}}) \stackrel{\text{def}}{=} \frac{\text{Area}(\mathbf{P}^{\text{PV}} \cap \mathbf{G}^{\text{PV}})}{\text{Area}(\mathbf{G}^{\text{PV}})}, \quad (6)$$

with $\text{Area}(\cdot)$ computing the area of a given polygon. More concretely, Fig. 3 illustrates our rationale. It can be observed that while IoU indicates the degree of alignment, IoGT reflects the degree of enclosure and better serves the purpose of the PV constraint. Consequently, IoGT maximizes at 1 when the prediction \mathbf{P}^{PV} fully encloses the ground truth \mathbf{G}^{PV} .

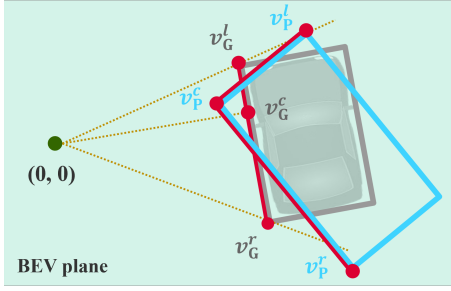


Fig. 4: An example showing the risk where with the prediction’s closest point v_P^c placed closer than the ground truth’s v_G^c , parts of the ground truth may still be exposed. Hence, we suggest taking into account the entire AV-facing sides, which are defined by the right-most and left-most corners from the AV’s perspective.

Now, with the PV constraint and its quantitative measure formulated, there is another risk that may be neglected: Even when $\Pi^{\mathcal{PV}}$ in Eq. (5) is satisfied, it is still possible that in the 3D world, the ground truth \mathbf{G} is not fully covered by the prediction \mathbf{P} from the AV’s location. For instance, the prediction \mathbf{P} might be farther from the AV yet much larger than the ground truth \mathbf{G} , so that after the perspective projection, $\mathbf{P}^{\mathcal{PV}}$ indeed encloses $\mathbf{G}^{\mathcal{PV}}$. To prevent such cases, we need to consider the depth information, or distance underestimation to be specific, in the BEV plane.

B. Distance Underestimation in the BEV Plane

As motivated, a rule of thumb in the BEV plane is that the prediction should be no farther than the ground truth. We provide a precise definition and a quantitative measure in the following.

First, as in the PV plane, we need the projected bounding boxes in the BEV plane. To such end, we perform an orthographic projection on the prediction \mathbf{P} and the ground truth \mathbf{G} . Since we have assumed upright 3D bounding boxes, an orthographic projection simply boils down to taking the BEV attributes from the 3D representations, e.g., $(x_G, z_G, l_G, w_G, \theta_G)$ for the ground truth \mathbf{G} , and then the BEV bounding boxes can be reconstructed. In the following, we denote the projected prediction as $\mathbf{P}^{\mathcal{BEV}}$ and ground truth as $\mathbf{G}^{\mathcal{BEV}}$.

For assessing the prediction $\mathbf{P}^{\mathcal{BEV}}$, the prior art [11] has suggested considering the closest-point distance rather than the center distance [1], especially in safety-critical situations. We take the same rationale and denote the point closest to the AV in the ground truth as v_G^c and the one in the prediction as v_P^c . Then, the requirement of closest-point distance underestimation can be specified as:

$$\Pi_c^{\mathcal{BEV}} \stackrel{\text{def}}{=} \|v_P^c\| \leq \|v_G^c\|, \quad (7)$$

where $\|\cdot\|$ here denotes the point distance to the origin.

That said, we note a pitfall where $\Pi_c^{\mathcal{BEV}}$ is satisfied but some part of the ground truth $\mathbf{G}^{\mathcal{BEV}}$ is still exposed, as depicted in Fig. 4. It shows that for full coverage over the ground truth $\mathbf{G}^{\mathcal{BEV}}$, one has to consider the entire side(s) facing the AV. Hence, we utilize the extreme points of $\mathbf{P}^{\mathcal{BEV}}$

and $\mathbf{G}^{\mathcal{BEV}}$ from the AV’s perspective and further ensure there is no intersection in these sides. Formally, we define now the BEV constraint as:

$$\Pi^{\mathcal{BEV}} \stackrel{\text{def}}{=} \Pi_c^{\mathcal{BEV}} \wedge \neg \perp(\{v_P^c v_P^r, v_P^c v_P^l, v_G^c v_G^r, v_G^c v_G^l\}), \quad (8)$$

where v_G^r and v_G^l denote the right-most and left-most corners in the ground truth $\mathbf{G}^{\mathcal{BEV}}$ from the AV’s perspective (similarly for the prediction $\mathbf{P}^{\mathcal{BEV}}$), and $\perp(\cdot)$ is a function that checks if a given set of line segments has an intersection, excluding overlapping endpoints. In practice, the function $\perp(\cdot)$ can be implemented by the Sweep Line Algorithm [15].

For the quantitative measure in the BEV plane, we observe generally that the farther the prediction is placed from the AV in comparison to the ground truth, the larger a portion of the ground truth is exposed. Therefore, we leverage the defined representative points (i.e., the closest, left-most, and right-most points from the AV’s perspective) and formulate an average distance ratio (ADR) as follows:

$$\text{ADR}(\mathbf{P}^{\mathcal{BEV}}, \mathbf{G}^{\mathcal{BEV}}) \stackrel{\text{def}}{=} \left(\prod_{i=\{c,r,l\}} \frac{\|v_G^i\|}{\max(\|v_P^i\|, \|v_G^i\|)} \right)^{(1/3)}. \quad (9)$$

Essentially, we compute individually how far the prediction’s representative points are from the AV compared to their ground truth counterparts and aggregate the point-wise ratio by taking the geometric mean. Here, using the geometric mean instead of other central tendencies, such as the arithmetic mean, gives more robust results, e.g., in the case of a large prediction [16]. Lastly, similar to IoGT, which maximizes when the prediction arrives at a “safe” state, ADR also saturates at 1 if the prediction’s points are all closer than their corresponding ground truth points.

C. Consolidation for Model Evaluation

So far, we have discussed the PV and BEV constraints as well as their quantification separately. To generate a verdict for a prediction \mathbf{P} with the ground truth \mathbf{G} in the 3D world, we consolidate the uncompromising spatial constraints (USC) from Eq. (5) and Eq. (8) as:

$$\Pi_{\text{USC}} \stackrel{\text{def}}{=} \Pi^{\mathcal{PV}} \wedge \Pi^{\mathcal{BEV}}. \quad (10)$$

Thereby, we obtain a qualitative indicator checking if the prediction \mathbf{P} fully covers the ground truth \mathbf{G} when seen from the AV. In addition, with the formulated PV and BEV quantitative measures in Eq. (6) and Eq. (9), we can produce a scoring function as:

$$\text{USC}(\mathbf{P}, \mathbf{G}) \stackrel{\text{def}}{=} \text{IoGT} \times \text{ADR}, \quad (11)$$

where we omit the notation of the projected PV and BEV bounding boxes for simplicity. Generally, a prediction \mathbf{P} gets a higher USC score if it covers the ground truth \mathbf{G} better. Since both IoGT and ADR range from 0 to 1, the overall score also ranges over $[0, 1]$.

As seen, USC is designed as a TP measure to examine a pair of matched prediction \mathbf{P} and ground truth \mathbf{G} . After examining the matched pairs for an object class, we can calculate an *average USC (AUSC)*. Then, summarizing the results from all object classes gives the *mean AUSC (mAUSC)*. Furthermore, to also reflect FP and FN predictions, we follow the nuScenes protocol, which incorporates already the recall-precision-based mAP metric, and simply extend mAUSC as follows:

$$\text{USC-NDS} = \frac{1}{2}[\text{NDS} + \text{mAUSC}]. \quad (12)$$

As such, USC-NDS not only reflects the general object detection performance but also characterizes our safety-oriented spatial constraints from the driving perspective. To see their efficacy, we shall use the consolidated AUSC, mAUSC and USC-NDS for model evaluation in our experiments later.

V. SAFETY-ORIENTED FINE-TUNING

Apart from examining model performance with the safety-oriented spatial constraints, we consider how to improve them via a loss function for continual learning. In particular, along with our analysis, we notice that an ultimate safety-oriented goal in AD is to encapsulate the ground truths with predictions. That is, while the spatial constraints tolerate certain errors and require a prediction to cover the ground truth from the AV’s perspective, we directly aim for proper containment with the 3D bounding boxes during optimization.

It turns out that a proper containment can be modeled by the 3D version of the IoGT function, comparing volumes of the intersection $\mathbf{P} \cap \mathbf{G}$ and ground truth \mathbf{G} , similar to Eq. (6). The better a prediction contains the ground truth, the higher its IoGT score. With a full containment, IoGT maximizes at 1. Therefore, we compose an IoGT loss as:

$$L_{\text{IoGT}} \stackrel{\text{def}}{=} 1 - \text{IoGT}(\mathbf{P}, \mathbf{G}). \quad (13)$$

Nevertheless, the IoGT loss by itself does not provide a complete solution, since it vanishes when the prediction over-approximates the ground truth. We consequently combine it with accuracy-guided loss functions such as the SmoothL1 loss (L_{SmoothL1}) [17] and obtain a safety-oriented loss function:

$$L_{\text{safety}} \stackrel{\text{def}}{=} \lambda \cdot L_{\text{SmoothL1}} + (1 - \lambda) \cdot L_{\text{IoGT}}, \quad (14)$$

where $\lambda \in \mathbb{R} : 0 < \lambda < 1$ is a balancing parameter. In practice, similar to the NN learning rate, λ can be tuned during a learning session to favor accuracy in early episodes and improve safety-related performance at later stages.

VI. EXPERIMENTS

With the proposed USC-based metrics for model evaluation in Sec. IV-C and the safety-oriented loss function for model fine-tuning in Sec. V, we now conduct experiments to answer the following three research questions (RQs).

- RQ1: Given their generally good performances, how do state-of-the-art models perform in terms of the safety-oriented USC-based metrics?

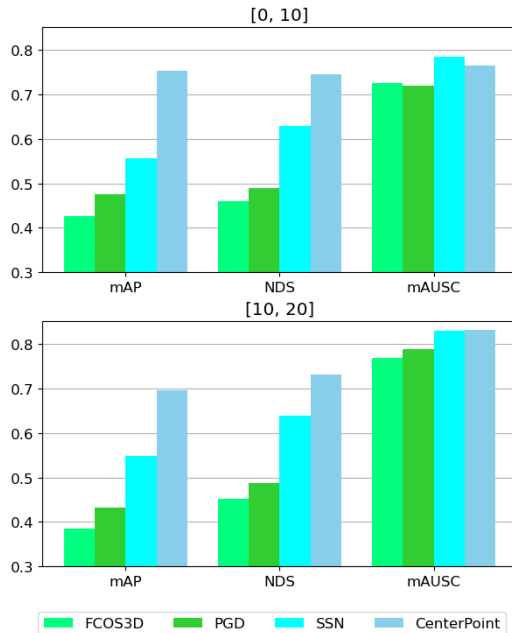


Fig. 5: Range-based model evaluation results. The upper plot shows the scores of the four examined models for objects ranging in [0, 10] meters, and the lower [10, 20] meters. The camera-based FCOS3D [18] and PGD [19] are plotted in green, and the lidar-based SSN [20] and CenterPoint [21] are in blue.

- RQ2: Can the proposed loss function improve the model’s performances, especially regarding the safety-oriented scores?
- RQ3: Ultimately, are USC-based metrics better performance indicators for system safety?

The RQs will be investigated in the following three sections respectively.

A. Model Evaluation

We now start with RQ1 and evaluate various models in terms of the existing accuracy-based mAP and NDS as well as our USC-based metrics.

1) *Implementation*: We utilize object detectors hosted on the MMDetection3D platform [22], specifically the top-performing lidar-based models SSN [20] and CenterPoint [21] as well as camera-based ones FCOS3D [18] and PGD [19]. The MMDetection3D platform also has an interface connecting the nuScenes dataset, which defines the evaluation protocol [1] introduced in Sec. III.

Given our safety-oriented considerations for collision avoidance, we make several adaptations on the nuScenes protocol. First, we concentrate on objects within 20 meters, instead of 50. Then, we separate the objects by their ranges to give a more detailed analysis. For objects within 0 to 10 meters, we tighten the TP threshold from 2 to 1 meter. Lastly, some object classes do not exist in specific ranges. For example, no construction vehicles are situated within [0, 10] meters in all scenes. For such cases, the original nuScenes protocol assumes the worst scores, e.g., 0 AP and full TP errors, leading to overly underestimated performance.

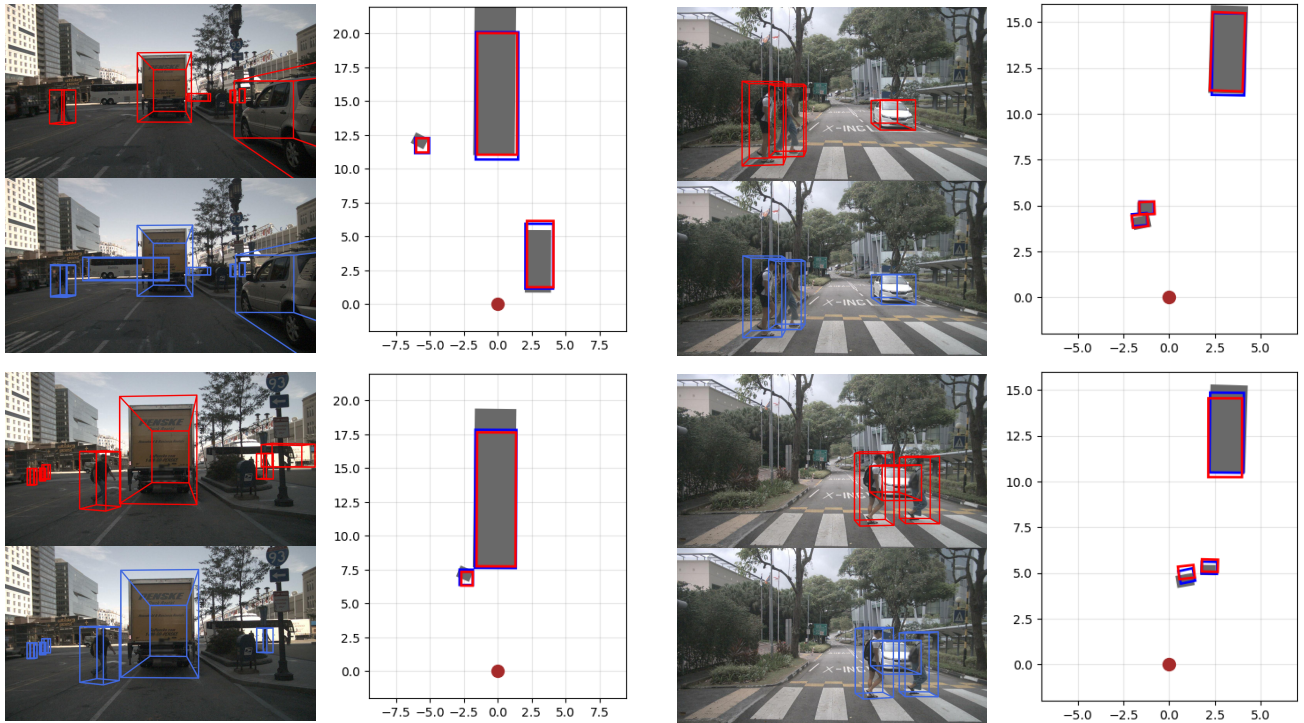


Fig. 6: Qualitative fine-tuning results of the camera-based PGD model [19]. We provide samples from two driving scenarios (organized column-wise), each with two time steps. For each time step, the upper left image shows red predictions based on $L_{SmoothL1}$ [17], the lower left image shows blue predictions based on our L_{safety} , and on the right is a BEV projection of all predictions alongside the ground truths in gray.

TABLE I: Quantitative fine-tuning results of the camera-based PGD model [19].

Model	Modality	NDS (%)	mAUSC (%)	Pedestrian		Car		Truck	
				ATE (\downarrow)	AUSC (\uparrow)	ATE (\downarrow)	AUSC (\uparrow)	ATE (\downarrow)	AUSC (\uparrow)
PGD [19]	Camera	50.76	75.35	0.439	0.728	0.326	0.811	0.498	0.803
+ $L_{SmoothL1}$ [17]	Camera	50.68 (-0.2%)	75.69 (+0.5%)	0.433	0.729	0.325	0.804	0.497	0.794
+ L_{safety} (ours)	Camera	50.88 (+0.2%)	78.54 (+4.2%)	0.434	0.732	0.324	0.813	0.503	0.805

Finding that sub-optimal, we do not account for missing classes in our experiments.

2) *Results and Discussions:* We plot the evaluation results of the four models in Fig. 5, where we observe the safety-oriented performance of the models does not necessarily follow the same trend as their accuracy-based performance. We elaborate on the observation with the following three points.

First, while there are large accuracy gaps between camera-based and lidar-based models, the gaps in terms of mAUSC are much smaller. This likely shows that when it comes to localizing nearby objects and covering them with “safe” enough predictions, the camera-based models are not as bad as indicated by the accuracy-based metrics.

Second, looking at the plot for $[0, 10]$ meters, the mAUSC score of PGD is actually lower than that of FCOS3D, despite it having higher mAP and NDS. A similar situation appears for the lidar-based CenterPoint and SSN. This finding resonates with the related work [10], pointing out that more accurate models may still exhibit safety concerns in nearby ranges.

Third and lastly, from the $[0, 10]$ range to the $[10, 20]$

range, the mAP and NDS of the models tend to drop, while their mAUSC interestingly increase. This may be attributed to the error-tolerating principles when designing mAUSC. Essentially, the objects at a distance tend to be harder to localize, but it may be fine so long as the predictions cover the ground truths (as exemplified by Fig. 1).

Altogether, the model evaluation results using mAP, NDS, and our USC-based metrics demonstrate that state-of-the-art models may have different safety-oriented performance from what is generally perceived.

B. Model Fine-Tuning

In this section, we continue with RQ2. In particular, considering the potential safety concern of PGD discovered in RQ1, we apply the safety-oriented loss function for it.

1) *Implementation:* Since the PGD object detector originally outputs a unique image-based representation of the 3D bounding boxes, we append to it a transformation function and obtain the typical representation (as shown in Sec. III). Then, together with the annotated ground truths, the IoGT loss and safety-oriented loss (with λ set to 0.8) can be calculated. We run five fine-tuning sessions for the best

PGD checkpoint provided on MMDetection3D [22] using the same learning configurations as the original PGD work, e.g., NN learning rate and data augmentation policy. For comparison, we also run five sessions with the accuracy-guided loss function $L_{S_{\text{smoothL1}}}$. All sessions are run with a batch size of six samples for six epochs of a subset shared by the nuScenes benchmark [1]. Each session takes roughly two hours on an Nvidia RTX A6000.

2) *Results and Discussions:* We present in Tab. I the fine-tuning results, which are the average of the five sessions for the $L_{S_{\text{smoothL1}}}$ -based models and the L_{safe} -based models respectively. We also provide qualitative samples from two driving scenarios, each with two time steps, in Fig 6.

Interestingly, as Tab. I shows, the proposed loss function not only improves the model’s safety-oriented performance in terms of mAUSC but also maintains, or even slightly increases, the accuracy-based NDS. This likely stems from the explicit usage of IoGT in the loss function, which attempts not only to ensure full coverage but to encapsulate the ground truth entirely, thereby keeping the predictions aligned at the same time. The effect is visualized in the qualitative samples, where most of the blue predictions contain the ground truths to a larger extent and are aligned well.

Regarding the class-specific results, a similar trend can be observed too. For example, corresponding to the higher pedestrian AUSC achieved by L_{safe} , the pedestrians are better captured by the blue predictions shown at the lower instance of the right scenario in Fig. 6.

Overall, the proposed loss function does increase the model’s performances, especially in terms of the safety-oriented scores. Although the improvement might be marginal, such differences may play an important role when it comes to safety-critical situations. For further enhancement, nonetheless, one may consider adopting related approaches such as box enlarging in a post-processing fashion [3], [4].

C. Closed-Loop Validation

Finally, in this section, we explore RQ3 and validate the proposed safety-oriented USC-based metrics with a system-level simulation. In principle, to be indicative and effective, a model-level metric should have a good correlation with the actual system-level testing result.

1) *Implementation:* We run all the baseline and fine-tuned camera-based object detectors on an AV equipped with an automatic braking function (AEB) in the Prescan simulator. For each of the twelve models (two baselines and ten fine-tuned), we repeat 100 simulations. Then, we compute the Pearson correlation coefficients between the model-level metrics and the AV collision rates.

To briefly explain, in every simulation, the AV’s mission is to perform valet parking by driving along a designated path from a hand-off zone to a parking slot. During the mission, a pedestrian will cross the driveway, thereby testing the object detection and AEB functions of the AV. The AEB function operates based on a simple rule: If an object is detected within the braking range of the AV, it will take a



Fig. 7: The system-level simulation setup: (Top) The gray AV equipped with the object detector and AEB function is commissioned to drive from the yellow hand-off zone to the green parking slot. (Bottom) During the mission, the pedestrian at the back (e.g., an old man here) crosses the driveway and causes a collision potentially.

TABLE II: Absolute Pearson correlation coefficients between model-level metrics and the simulated system-level collision rates.

Metric	Correlation
mAP (mean Average Precision)	0.699
NDS (NuScenes Detection Score)	0.806
mAUSC (mean Average USC)	0.814
USC-NDS (an average of the above two)	0.925

full brake. Hence, whether a collision occurs depends mainly on the object detector’s performance. Lastly, for more diverse testing, we alter the pedestrian types, speed, crossing timing, and environmental conditions such as illumination. Fig. 7 illustrates the setup. Readers can check our demonstration video [23] or Sec. 4.2 of an overviewing project paper [24] for more details regarding the AV’s simulation and testing.

2) *Results and Discussions:* Generally, we see the fine-tuned PGD models with higher safety-oriented scores lead to fewer simulation collisions. Tab. II summarizes the results with the Pearson correlation coefficients. For clarity, we report the absolute values so that the higher the value, the more indicative the model-level metric.

It can be observed that compared to the conventional mAP, NDS already reflects the system-level performance well. This is similarly concluded in the recent validation work [9]. Nonetheless, the proposed mAUSC outperforms NDS, and by combining the two, one can attain the most indicative model-level metric for the system-level collision rates.

To reflect on the results, we find that in most simulations, the pedestrians are detected (as in Fig. 6), and mAUSC successfully characterizes the safety-oriented properties in these cases. Still, there are simulations where the pedestrians are not detected at all, and considering these cases, the well-rounded USC-NDS metric is indeed the most suitable proxy for system-level performance, as shown.

VII. CONCLUSION

In this work, observing the urge for appropriate performance indicators for 3D object detectors, we formulated uncompromising spatial constraints (USC) and corresponding quantitative metrics based on a safety point of view. Concretely, given a prediction \mathbf{P} and its targeted ground truth \mathbf{G} , the proposed USC require the prediction \mathbf{P} to cover the ground truth \mathbf{G} when seen from the AV. Such a requirement foregoes the likely unachievable perfect detection demanded by conventional accuracy-based metrics such as mAP. We conducted extensive experiments with the nuScenes datasets and a closed-loop AEB system simulation. The results demonstrated the efficacy of USC-based metrics in finding safety-oriented and more dependable models as well as its potential to gear existing models towards better performances beyond pure accuracy.

On a broader scope, our investigation joins the recent efforts in AD safety engineering and puts forth a promising proposal for 3D object detectors. To proceed, there are several open directions. First, with the direct safety-oriented criterion, we plan to employ analytical or statistical approaches to get a reasonable performance threshold for deployment. Second, one may extend USC's usage in facilitating more advanced motion planning algorithms for smoother and safer maneuvers. Last but not least, how to adapt USC for run-time monitoring constitutes another interesting avenue.

REFERENCES

- [1] H. Caesar, V. Bankiti, A. H. Lang, S. Vora, V. E. Liong, Q. Xu, A. Krishnan, Y. Pan, G. Baldan, and O. Beijbom, "nuScenes: A multimodal dataset for autonomous driving," in *CVPR*, 2020.
- [2] "Artificial Intelligence Act," <https://eur-lex.europa.eu/legal-content/EN/TXT/?uri=celex%3A52021PC0206>, 2021.
- [3] F. de Grancey, J.-L. Adam, L. Alecu, S. Gerchinovitz, F. Mamalet, and D. Vigouroux, "Object detection with probabilistic guarantees: A conformal prediction approach," in *SafeComp Workshops*, 2022.
- [4] T. Schuster, E. Seferis, S. Burton, and C.-H. Cheng, "Unaligned but safe - Formally compensating performance limitations for imprecise 2D object detection," in *SafeComp*, 2022.
- [5] Z. Zou, K. Chen, Z. Shi, Y. Guo, and J. Ye, "Object detection in 20 years: A survey," *Proc. IEEE*, 2023.
- [6] C.-H. Cheng, "Safety-aware hardening of 3D object detection neural network systems," in *SafeComp*, 2020.
- [7] M. Lyssenko, P. Pimplikar, M. Bieshaar, F. Nozarian, and R. Triebel, "A safety-adapted loss for pedestrian detection in automated driving," 2024.
- [8] J. Philion, A. Kar, and S. Fidler, "Learning to evaluate perception models using planner-centric metrics," in *CVPR*, 2020.
- [9] T. Schreier, K. Renz, A. Geiger, and K. Chitta, "On offline evaluation of 3D object detection for autonomous driving," 2023.
- [10] B. Deng, C. R. Qi, M. Najibi, T. Funkhouser, Y. Zhou, and D. Anguelov, "Revisiting 3D object detection from an egocentric perspective," in *NeurIPS*, 2021.
- [11] K. T. Mori and S. Peters, "SHARD: Safety and human performance analysis for requirements in detection," *T-IV*, 2024.
- [12] N. Ravi, J. Reizenstein, D. Novotny, T. Gordon, W.-Y. Lo, J. Johnson, and G. Gkioxari, "Accelerating 3D deep learning with PyTorch3D," 2020.
- [13] R. I. Hartley and A. Zisserman, *Multiple View Geometry in Computer Vision*. Cambridge University Press, 2004.
- [14] L. Liu, J. Lu, C. Xu, Q. Tian, and J. Zhou, "Deep fitting degree scoring network for monocular 3d object detection," in *CVPR*, 2019.
- [15] D. Souvaine, "Line segment intersection using a sweep line algorithm," 2005.
- [16] P. J. Fleming and J. J. Wallace, "How not to lie with statistics: The correct way to summarize benchmark results," *Commun. ACM*, 1986.
- [17] W. Liu, D. Anguelov, D. Erhan, C. Szegedy, S. Reed, C.-Y. Fu, and A. C. Berg, "SSD: Single shot multibox detector," in *ECCV*, 2016.
- [18] T. Wang, X. Zhu, J. Pang, and D. Lin, "FCOS3D: Fully convolutional one-stage monocular 3D object detection," in *ICCVW*, 2021.
- [19] —, "Probabilistic and geometric depth: Detecting objects in perspective," in *CoRL*, 2021.
- [20] X. Zhu, Y. Ma, T. Wang, Y. Xu, J. Shi, and D. Lin, "SSN: Shape signature networks for multi-class object detection from point clouds," in *ECCV*, 2020.
- [21] T. Yin, X. Zhou, and P. Krähenbühl, "Center-based 3D object detection and tracking," *CVPR*, 2021.
- [22] MMDetection3D Contributors, "MMDetection3D: OpenMMLab next-generation platform for general 3D object detection," <https://github.com/open-mmlab/mmdetection3d>, 2020.
- [23] "EU Horizon 2020 FOCETA Project: Demonstrating safety assurance for an automated valet parking system," <https://drive.google.com/file/d/1oSAXAyVShGksclCHyqLH8BKigRvuLWej/view?usp=sharing>, 2023.
- [24] S. Bensalem, P. Katsaros, D. Ničković, B. H.-C. Liao, R. R. Nolasco, M. A. E. S. Ahmed, T. A. Beyene, F. Cano, A. Delacourt, H. Esen, A. Forrai, W. He, X. Huang, N. Kekatos, B. Könighofer, M. Paulitsch, D. Peled, M. Ponchant, L. Sorokin, S. Tong, and C. Wu, "Continuous engineering for trustworthy learning-enabled autonomous systems," in *AISoLa*, 2023.